Single-Cell RNA Sequencing Profiling Cellular Heterogeneity and Specific Responses of Fish Gills to Microplastics and Nanoplastics

Zheng, Siwen; Wang, Wen-Xiong

Published in:
Environmental Science and Technology

Published: 02/04/2024

Document Version:
Post-print, also known as Accepted Author Manuscript, Peer-reviewed or Author Final version

Published version (DOI):
10.1021/acs.est.3c10338

Publication details:
Zheng, S., & Wang, W.-X. (2024). Single-Cell RNA Sequencing Profiling Cellular Heterogeneity and Specific Responses of Fish Gills to Microplastics and Nanoplastics. *Environmental Science and Technology*, *58*(13), 5974-5986. https://doi.org/10.1021/acs.est.3c10338

Single-Cell RNA Sequencing Profiling Cellular Heterogeneity and Specific Responses of Fish Gills to Microplastics and Nanoplastics

Siwen Zheng [a,b], Wen-Xiong Wang [a,b,*]

[a] *School of Energy and Environment and State Key Laboratory of Marine Pollution, City University of Hong Kong, Kowloon, Hong Kong, China*

[b] *Research Centre for the Oceans and Human Health, City University of Hong Kong Shenzhen Research Institute, Shenzhen 518057, China*

*Corresponding author: wx.wang@cityu.edu.hk

ABSTRACT

Fish gills are highly sensitive organs for microplastics (MPs) and nanoplastics (NPs) invasions, but the cellular heterogeneity of fish gills to MPs and NPs remains largely unknown. We employed single-cell RNA sequencing (scRNA-seq) to investigate the responses of individual cell populations in tilapia *Oreochromis niloticus* gills to MPs and NPs exposure at an environmentally relevant concentration. Based on the detected DEGs numbers, the most affected immune cell by MPs exposure was macrophages, while the stimulus of NPs primarily targeted T cells. In response to MPs and NPs, H^+-ATPase-rich cells exhibited distinct changes as compared with Na^+/K^+-ATPase-rich cells and pavement cells. Fibroblasts were identified as a potential sensitive cell-type biomarker for MPs interaction with *O. niloticus* gills, as evidenced by the largely reduced cell counts and the mostly detected DEGs among the 12 identified cell populations. The most MPs sensitive fibroblasts subpopulation in *O. niloticus* gills was lipofibroblasts. Cell-cell communications between fibroblasts and H^+-ATPase-rich cells, neurons, macrophages, neuroepithelial cells, Na^+/K^+-ATPase-rich cells in *O. niloticus* gills were significantly inhibited by MPs exposure. Collectively, our study demonstrated cellular heterogeneity of *O. niloticus* gills to MPs and NPs and provided sensitive markers for their toxicological mechanisms at the single cell resolution.

KEYWORDS:

scRNA-seq; *microplastics*; *fish gill*; *heterogeneity responses*; *fibroblast*; *biomarker*

SYNOPSIS:

scRNA-seq reveals immune and physiological heterogeneities of *O. niloticus* gills to MPs and NPs, highlighting fibroblasts as a potential sensitive cell-type biomarker.

TOC (prepared by the authors)

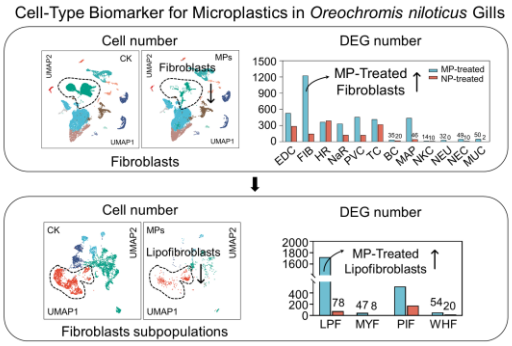

INTRODUCTION

Widespread plastic products in our daily life have recently surged to the forefront of environmental concerns on a global scale. [1-3] Improper disposal of plastic products can lead to massive microplastics (MPs) contamination in aquatic environments. [4] It was estimated that 19 to 23 million metric tons (Mt) of plastic waste were transported into aquatic ecosystems in 2016 and such value is predicted to reach up to 53 Mt annually by 2030. [5] MPs in aquatic ecosystems can inevitably be consumed by fish [6] and transferred to humans, [7] subsequently posing high risks of human disease. [8] It is thus crucial to investigate the impacts of MPs on fish. MPs differ from traditional organic pollutants due to their various sizes and shapes, complex surface properties, and fragmentation potentials (to smaller sizes of plastic particles, e.g., nanoplastics, NPs). [9] In prior studies, the toxicological endpoints of MPs in fish have been widely elucidated, including neurotoxicity, [10] reproductive impairment, [11] liver damage, [12] intestinal microbial disorder, [13] and beyond. However, biomarker for MP-specific toxicity testing for fish remains largely unknown.

Digestive organs (e.g., gut and intestines) are widely recognized as the primary target for the accumulation of MPs in fish. [14, 15] In recent years, a previously overlooked but MP-sensitive organ (i.e., gill) in fish has yet attracted increasing attention. It was demonstrated that the proportion of the retained polystyrene (PS) in gills of medaka *Oryzias melastigma* can reach more than 10%. [16] When compared to muscles and internal organs, fish gill has direct contact with the surrounding water; sampling of which causes less harm and is thus considered a less invasive method for monitoring health status of fish in aquaculture. [17] This makes gill an ideal organ for studying MPs biomarker in fish. Additionally, fish gill performs essential immune and physiological functions; disturbance of which might pose a huge threat to fish health. [18] However, research on the impacts of MPs on fish gill is still limited. Imbalances in ion regulation and ammonia excretion were reported in medaka *O. melastigma* upon the exposure to MPs, as evidenced by the co-altered bacterial community through the gut-gill axis. [19] The influence of MPs on respiratory function of tilapia *Oreochromis niloticus* was also recognized based on the differential expression of genes and metabolites detected in the gills. [20] More specific responses and toxicological mechanisms of fish gills to MPs need to be thoroughly characterized.

Single cell RNA sequencing (scRNA-seq) has recently emerged as a powerful tool for studying the heterogeneity responses of aquatic organisms in response to external stimulus in environmental toxicological studies. [21, 22] Traditional bulk RNA-seq methods provide cell

population-averaged gene expression profiles of the whole tissue to the changing environmental conditions. [23, 24] Based on such measurements, the large fold changes in gene expression of the responsive cells would be overshadowed by other insensitive cells, leading to inaccurate results. In contrast, scRNA-seq allows for the characterization of individual cells within a tissue, shedding light on the intricate cellular heterogeneity and specific responses to environmental pollutants. [25, 26] For example, heterogeneity effects of bisphenol A (BPA) to zebrafish embryos at different developmental stages were previously examined using scRNA-seq and results showed that BPA primarily changed gene expression of enveloping layer cells of zebrafish embryos at 8 hpf, but affected neural crest cells and forebrain cells at 12 hpf and 30 hpf respectively. [27] In addition, scRNA-seq analysis based on zebrafish intestines revealed that only NPs altered expression of genes associated with phagocyte-produced reactive oxygen species generation, while MPs specifically affected the processes involved with lysosome and cell surface receptor signaling in macrophages. [28] The scRNA-seq technique represents a significant advancement in environmental toxicology, offering unprecedented insights into the cellular-level impacts of pollutants (like MPs) within a tissue.

To analyze the heterogeneous responses of MPs to fish gills and further identify their potential sensitive biomarker, scRNA-seq was conducted based on the gill samples collected from tilapia *O. niloticus* after MPs exposure. NPs are distinguished from MPs due to their different transportation processes and surface properties, [29] therefore *O. niloticus* gills treated with NPs were also conducted for scRNA-seq analysis as comparison. Immune and physiological heterogeneity responses of *O. niloticus* gills to MPs and NPs were fully profiled and the subsequent enrichment analysis was performed to decipher the potential toxicological mechanisms. This study clearly illustrated the heterogeneous endpoints for MPs and NPs interaction with *O. niloticus* gills based on bioinformatics analysis at the single cell level. Our results enhance the understanding of toxicological mechanisms of fish gills to MPs and NPs, thereby mitigating potential environmental risks.

MATERIALS AND METHODS

Synthesis and Characterization of MPs and NPs. To examine the uptake of MPs and NPs in *O. niloticus* gills, aggregation-induced emission fluorogens (AIEgens) labelled PS particles (AIE-MPs, 20 μm and AIE-NPs, 80 nm) were synthesized and employed in this study, due to their excellent fluorescence properties, biocompatibility, and physical stability

produced by AIEgens. [30] Synthesis of AIE-MPs and AIE-NPs was based on previous studies [31, 32] by batch emulsion polymerization using styrene (St), methyl methacrylate (MMA), and acrylic acid (AA). AIEgens purchased from AIEgen Biotech Co., Ltd. (Guangzhou, China) were added as the chemical dye and embedded within the synthesized PS-P(MMA-AA) core-shell structure. To prevent shedding of the unbound AIEgens, the synthesized AIE materials were rinsed three times with Milli-Q water and transferred to a dialysis bag (1 kDa) for five days before use. [33] Given the time and economic costs, the same size of pristine MPs (20 μm) and NPs (80 nm) without fluorescent agents purchased from Tianjin BaseLine ChromTech Research Centre (Tianjin, China) were used for additional exposure experiments in this study. The additives (e.g., sodium dodecyl sulfate) in the stock solution of the commercial pristine MPs and NPs were removed by filtering through a 10 kDa regenerated cellulose ultrafiltration membrane based on a previous study before use. [34] The particle size and surface morphology for each particle were characterized by scanning electron microscope (SEM, Zesis EVO MA10, USA). The hydrodynamic diameters of these particles in the culture water were monitored using laser diffractometer (Mastersizer 3000, Malvern, UK) for MPs and Zetasizer (Nano ZS, Malven, UK) for NPs. Zeta potentials for these particles were measured using Zetasizer (Nano ZS, Malven, UK). PL spectra of the synthesized AIE-MPs and AIE-NPs were measured by luminescence spectroscopy (LS 55, PerkinElmer, USA).

Fish Maintenance. Healthy tilapia larvae (*O. niloticus*, 3.5–4.0 cm in total length) were collected from a local aquaculture farm (Guangzhou, China) with excellent *O. niloticus* culturing experience for more than five years. *O. niloticus* with similar sizes were acclimated in five 60-L glass tanks (60 *O. niloticus* per tank) with continuous circulation and aeration of dechlorinated tap water at 25 ± 1 °C in a 14 h/10 h light/dark cycle for more than two weeks. During the acclimatization period, the *O. niloticus* were fed with commercial food pellets (BIOZYM, China) twice daily at 1% body weight. No deaths were observed for the two weeks prior to the formal experiments. All animal experiments in this study were performed in accordance with the guidelines approved by the Animal Research Ethics Committee of City University of Hong Kong.

Fish Exposure to MPs and NPs. The exposure concentration of MPs and NPs in this study was 100 μg/L. This concentration was widely employed as environmentally relevant exposure concentration in previous toxicity studies. [10, 35] For 20 μm MPs, 100 μg/L was equivalent to 22,727 particles/L, which was within the reported range of MPs across 98 lakes worldwide (0.27−34,000 particles/L). [36] The count of 80 nm NPs at 100 μg/L was equivalent

to 3.55E+11 particles/L. After starving for 48 h, the acclimated *O. niloticus* were randomly assigned for two sets of 28-day exposure experiments following OECD guideline 210 [37] (experiment 1, AIE-MPs and AIE-NPs were employed to track the uptake of PS in *O. niloticus* gills; experiment 2, pristine MPs and NPs were exposed to *O. niloticus* for subsequent morphology analysis and scRNA-seq analysis aiming their gills). We have obtained control and two treatments for each set of exposure experiment (i.e., control, AIE-MPs, AIE-NPs for experiment 1; control, MPs, NPs for experiment 2). Three replicate 5-L fish tanks were set up per condition for experiment 1 and six replicate 5-L fish tanks were set up per condition for experiment 2. Six *O. niloticus* were placed in each tank. To keep constant exposure concentration of AIE-MPs and AIE-NPs over 28 days, the reduced concentration of the water medium was measured (based on fluorescence intensity, Cary Eclipse fluorescence spectrophotometer, Agilent, USA) every other day, and half of the water medium was renewed with fresh solution containing the required concentrations of AIE-MPs and AIE-NPs. Given the concentration of pristine MPs and NPs cannot be directly measured, equal concentration was employed for half refreshment of pristine MPs and NPs solution following AIE-MPs and AIE-NPs, respectively. To prevent MPs and NPs sinking, air bubbling was used in each tank.

After 28 days of exposure, the six *O. niloticus* were collected in each tank in experiment 1 and the six gills were pooled as a biological replicate (three replicates per condition) for PS semi-quantification based on fluorescence intensity. The collected gill samples were freeze-dried and digested in 10% potassium hydroxide (w/v) at 60 ℃ for 2 h before being analyzed by Cary Eclipse fluorescence spectrophotometer (Agilent, USA). The contents of AIE-MPs and AIE-NPs in the digestion solution were quantified based on standard curve developed between concentration gradients of AIE-MPs and AIE-NPs suspensions and their respective fluorescence intensities (detailed calculation provided in Text S1). Detection limit for AIE-MPs and AIE-NPs was below 1 μg/L. For experiment 2, one *O. niloticus* was randomly picked from the six tanks per condition and kept in 4% paraformaldehyde (n = 3) and 2.5% glutaraldehyde (n = 3) for histopathological analysis (details provided in Text S2) and transmission electron microscope (TEM) observation, respectively. Then, the left five *O. niloticus* were picked from three tanks as a replicate biological sample (two biological replicates per condition) and kept in DPBS solution (Solarbio, China) at 4 ℃ before subsequent scRNA sequencing.

TEM Observation. The collected gill tissues of *O. niloticus* were immersed in 2.5%

glutaraldehyde and fixed at 4 °C for 12 h. Then, the gill samples were mixed with 1% osmium tetroxide and dehydrated using acetone before being embedded in epoxy resin. The resin blocks were hardened at 60 °C for 48 h and then sectioned into 70 nm using Leica UC7 ultramicrotome (Leica Microsystems GmbH, Germany). After post-stained with aqueous uranyl acetate and lead citrate, the section samples were observed under TEM (Hitachi HT7700, Japan).

Tissue Dissociation and Cell Purification. The collected gill tissues of *O. niloticus* were digested using dissociation enzyme Trypsin (0.25%, Hyclone, USA) and DNase I (10 mg/L, Takara Bio, USA). The gill tissues were dissociated at 37 ℃ under the speed of 50 rpm for 40 min. The dissociated cells were collected repeatedly at interval of 20 min to increase cell yield and viability. The cell suspensions were filtered through a 40 μm nylon cell strainer and the red blood cells were removed using Red Blood Cell Lysis buffer (Thermo Fisher Scientific, USA) and the cell suspensions were filtered through a 40 μm nylon cell strainer. This method was reported to exert no impact on thrombocytes. [38] Cell viability of each sample was checked on Countstar fluorescence cell analyzer (Aber Instruments Ltd., UK). Before being sequenced, the cell viability for each sample was confirmed to be above 80%.

Library Preparation and Single-Cell RNA Sequencing. Approximately 9,000 cells for each sample were subjected to the 10 × Genomics Chromium system for Gel Beads-in-Emulsion (GEM) generation. Beads containing unique molecular identifiers (UMIs) and cell barcodes were loaded until close to saturation, ensuring that each cell was paired with a bead in a GEM. After being exposed to cell lysis buffer, the polyadenylated RNA molecules hybridized to the beads. Beads were then retrieved and placed into a single tube for reverse transcription. Libraries for sequencing were prepared by utilizing randomly interrupted whole-transcriptome amplification products to enrich the 3′ end of the transcripts connected with the cell barcode and UMI. All remaining procedures, including library construction, were performed according to the standard manufacturer's protocol (Chromium Single Cell 3′). The quantification of the sequencing libraries was carried out using a high sensitivity DNA Chip (Bioanalyzer 2100, Agilent, USA) and the Qubit High Sensitivity DNA Assay (Thermo Fisher Scientific, USA). Subsequently, the libraries were sequenced on NovaSeq6000 (Illumina, USA) with a target of 150 bp paired end reads. The sequencing and bioinformatic analysis were conducted on platform of Majorbio Co., Ltd (Shanghai, China).

Bioinformatics Analysis of the Single-Cell RNA Sequencing Database. Raw

sequencing data were processed with Cell Ranger (v7.0.0, 10× Genomics) software for quality control. The resulting reads were aligned to the *O. niloticus* genome (GCF_001858045.2) using the STAR package. Gene-barcode matrices were generated for each sample by counting UMIs and filtering non-cell associated barcodes. The matrix was imported into the Seurat (v4.1.1) for quality control and downstream analysis of our scRNA-seq data. Low-quality cells were excluded from the matrices with the following three quality criteria: (1) number of UMIs ≤ 8000 per cell; (2) detected genes ranging from 500 to 4000 per cell; and (3) percent of reads mapping to mitochondrial genes ≤ 10%. The multidimensional dataset was visualized in a Uniform Manifold Approximation Projection (UMAP) graph showing similar expression of each cell cluster at a resolution of 0.2. Wilcoxon Rank-Sum Test was performed to find significant differentially expressed genes (DEGs) for each cell cluster over the remaining cell clusters with the following criteria: (1) *p*-adjust < 0.05; (2) $|\log_2 FC| \geq 0.25$ (FC, fold change, refers to fold difference in average expression between two groups); and (3) the percentage of cells in which the gene was detected in a specific cluster > 10%. After cell annotation, DEGs were also identified within one cell type under MPs and NPs exposure with the following criteria: (1) *p*-adjust < 0.05; (2) $|\log_2 FC| \geq 0.25$; and (3) the percentage of cells in which the gene was detected in a specific cluster > 10%. Gene Ontology (GO) and Kyoto Encyclopedia of Genes and Genomes (KEGG) enrichment analysis were performed using the identified DEGs, with significant enrichment set at *p*-adjust < 0.05.

Cell−Cell Communications. To investigate the cell−cell communications among the identified 12 cell populations in *O. niloticus* gills and characterize the differences between MPs and NPs treatments, the CellPhoneDB (v2.0) containing ligand−receptor information was applied to analyze the expression of ligand−receptor pairs. To create a ligand−receptor database, we constructed orthologous gene pairs between humans and *O. niloticus*, and only those with one-to-one relationship were retained for further analysis. [39] The significant ligand−receptor interactions were performed using CellPhoneDB method statistical analysis using our database and the default setting, with significant difference defined at *p*-value < 0.05.

Data Analysis. AIE-MPs and AIE-NPs contents of *O. niloticus* gills in the two treatments were corrected by reducing the autofluorescence detected in the control. Significant differences of AIE-MPs and AIE-NPs contents in *O. niloticus* gills between conditions were performed through one-way analysis of variance (ANOVA) followed by

Tukey's post-hoc test, with significance levels set at * $p < 0.05$, ** $p < 0.01$, and *** $p < 0.001$.

RESULTS

Uptake of MPs and NPs in *O. niloticus* Gills. To track the uptake of MPs and NPs in *O. niloticus* gills, the fluorescent PS particles AIE-MPs and AIE-NPs were synthesized by incorporating AIEgens in the inner side of PS particles. After synthesis, the AIE-MPs and AIE-NPs were observed under SEM and the results showed that the synthesized particles exhibited a near-spherical shape with an average size of 19.2 ± 0.3 μm and 78.4 ± 0.5 nm, respectively (Figure 1A). The hydrodynamic diameters of our synthesized AIE-MPs and AIE-NPs based on the culture water remained unchanged over continuous 96 hours (Figure 1B). Zeta potentials of AIE-MPs and AIE-NPs were −25.4 ± 0.9 mV and −29.5 ± 0.7 mV, respectively (Figure 1C). These results were comparable with those of the pristine PS particles with the same size (Figure 1) and the addition of the AIEgens did not cause significant alterations in the basic physicochemical properties of PS. The photoluminescence spectra of the synthesized AIE-MPs and AIE-NPs are shown in Figure 1D, with their strongest emission located at around 655 nm wavelength under excitation condition. After five days of filtration through 1 kDa dialysis bag, no fluorescent signal was detected in the leached solution of the AIE-MPs and AIE-NPs suspension, which indicates no significant dye leakage. The fluorescence signals of the AIE-MPs and AIE-NPs suspension remained highly stable over continuous 96 hours (Figure 1E). When compared to the commercial fluorescent PS particles without AIEgens, the detected fluorescence signals of AIE-MPs and AIE-NPs were ~8.7 and ~9.7 times higher under the same mass concentration, respectively (Figure S1).

During the 28-day uptake experiments, the spike concentration of AIE-MPs and AIE-NPs in each tank remained stable due to the constant addition of freshly prepared AIE-MPs and AIE-NPs suspension every other day (Figure S2). After 28-day exposure, the health status of *O. niloticus* was observed for each tank and no obvious abnormalities were found after AIE-MPs and AIE-NPs exposure. Furthermore, there were no significant differences in the total body length and weight of *O. niloticus* between the two treatments and the control (Table S1). AIE-MPs and AIE-NPs were significantly detected in *O. niloticus* gills and the AIE-MPs contents in *O. niloticus* gills were ~2.6 times higher than their AIE-NPs counterparts (Figure 2A), even if the particle number of AIE-NPs in the exposure medium

was much higher than that of AIE-MPs (when the particle mass is employed as the dose metric). Upon the uptake of MPs and NPs, tissue morphology of *O. niloticus* gills was studied. Based on TEM images, differential damages were observed after MPs and NPs exposure (Figure 2B). Specifically, after MPs exposure, mitochondria swelling and cristae fragmentation were observed, while NPs primarily induced chromatin marginalization and apoptosis in *O. niloticus* gills (Figure 2B). Based on the results of hematoxylin and eosin sections, significant aneurysms were observed in the MP-treated group, but not in the NP-treated group (Figure S3). The symptom of epithelial lifting and cell swelling was also less significant in the NP-treated group compared to the MP-treated group (Figure S3). Overall, the different morphology alterations observed between MP-treated and NP-treated groups warrant further investigation of their underlying mechanisms.

MPs and NPs Induced Distinct Cellular Transcriptome Profiles in *O. niloticus* Gills. To further reveal the impacts of MPs and NPs in *O. niloticus* gills, a total of 18,838, 20,350, and 14,543 cells were isolated from control, MP-treated, and NP-treated groups, respectively (two replicates per condition, six samples in total) for scRNA-seq analysis (Table S2). The resulting reads were aligned to the *O. niloticus* genome and the mapping rates ranged from 65.4% to 81.8% (Table S2). The sequence reads per cell for the six samples ranged from 28,632 to 46,641 (Table S2). A total of 53,731 cells were used for the following cell cluster analysis. After quality control, 33 cell clusters (clusters 0−32, Figure S4A) were obtained by dimensionality reduction and unsupervised cell cluster analysis. The top 3 enriched genes for each cell cluster were depicted in Figure S4B. The 33 clusters were then attributed to their putative cell identities based on the high expression of known markers (provided in Table S3) and functional characteristics. More detailed results of cell annotation for *O. niloticus* gills were reported previously. [40] In total, 12 cell populations were identified for *O. niloticus* gills, including endothelial cells (EDCs), fibroblasts (FIBs), ionocytes (i.e., H^+-ATPase-rich cells (HRs) and Na^+/K^+-ATPase-rich cells (NaRs)), immune cells (i.e., T cells (TCs), macrophages (MAPs), B cells (BCs), and natural killer cells (NKCs)), pavement cells (PVCs), neurons (NERs), neuroepithelial cells (NECs), and mucous cells (MUCs), as shown in Figure 2C. The top 10 highly enriched DEGs and selected signature genes for each cell population of *O. niloticus* gills are shown in Figure S5A and Figure S5B.

After 28-day exposure, no significant difference in cell clustering and cell annotation was observed between the two treatments and the control group (Figure S6 and Figure 2C). The total cell number of the 12 cell populations identified in *O. niloticus* gills increased by

8.0% after exposure to MPs, but decreased by 22.8% after exposure to NPs (Figure S7). The variation in cell number was cell type-specific under MPs and NPs exposure (Figure 2D). For the MP-treated group, six cell populations (including EDCs, PVCs, TCs, NaRs, NERs, and NECs) exhibited a significant increase in quantity as compared to the control, whereas five cell types (i.e., FIBs, HRs, MAPs, NKCs, and BCs) were inhibited significantly (Figure 2D). For the NP-treated group, a significant reduction of cell number was observed in EDCs, FIBs, MAPs, NKCs, and BCs, three of which belong to immune cells (Figure 2D). Only one cell type, HRs, exhibited a significantly higher cell count in the NP-treated group (Figure 2D). Additionally, significant cell number differences were observed for 11 cell populations (except MAPs) between MPs and NPs exposure (Figure 2D). Regarding DEGs, total number of the 12 identified cell populations in the MP-treated group was 2468 higher than that in the NP-treated group (Figure 2E). This finding aligned with our previous bulk RNA-seq data based on the cell population-averaged measurements (Figure S8). [20] Among the 12 identified cell populations, 11 of them showed more abundant DEGs in the MP-treated group than in the NP-treated group (Figure 2E), only except for HRs, exhibiting no significant difference.

Heterogeneous Responses of Immune Cells in *O. niloticus* Gills to MPs and NPs. Among the four immune cells (TCs, MAPs, BCs, and NKCs) of *O. niloticus* gills, only TCs count exhibited distinct responses to MPs and NPs (Figure 2D). Specifically, cell number of TCs increased by 57.8% under the stimulus of MPs, whereas exhibited no obvious change upon NPs exposure (Figure 2D). The co-altered DEGs by MPs and NPs exposure for each of the four immune cells are listed in Figure 3A. The potential markers for each immune cell in response to MPs and NPs were generated using the DEGs of the 12 identified cell types in *O. niloticus* gills (Figure S9) and the expression levels of representative markers for each immune cell are depicted in Figure 3B. Among the four immune cells in *O. niloticus* gills, the most detected DEGs by MPs exposure, was observed in MAPs, with an average of 439, whereas NPs exposure mostly changed gene expression in TCs (averaged 320) (Figure 2E and Figure 3A). For MP-treated group, anatomical structure formation involved in morphogenesis was significantly upregulated in MAPs (Figure 3C) and their DEGs were enriched in mitophagy, ras signaling pathway, and JAK-STAT signaling pathway (Figure 3D). For NP-treated group, significant downregulation of heme-copper terminal oxidase activity, cytochrome-c oxidase activity, and oxidoreductase activity was significantly observed in TCs (Figure 3C), and the enriched KEGG pathways included Th1 and Th2 cell differentiation, oxidative phosphorylation, and T cell receptor signaling pathway (Figure 3D).

Heterogeneity Responses of H^+-ATPase-Rich Cells, Na^+/K^+-ATPase-Rich Cells, and Pavement Cells in *O. niloticus* Gills to MPs and NPs. The stimulus of MPs enhanced cell numbers of NaRs and PVCs in *O. niloticus* gills by 1.4-fold and 2.1-fold, respectively, but reduced cell number of HRs by 37.5% (Figure 2D). On the contrary, NP exposure induced a 2.0-fold increase in count of HRs, but reduced cell numbers of NaRs and PVCs by 19.4% and 17.0%, respectively (Figure 2D). The common DEGs for HRs, NaRs, and PVCs in response to MPs and NPs are listed in Figure 4A. The expression levels of potential MP- and NP-responsive markers for HRs, NaRs, and PVCs in *O. niloticus* gills can be found in Figure 4B. Among HRs, NaRs, and PVCs, MPs induced the most DEGs in PVCs (averaged 457) (Figure 2E), with GO functions of transition metal ion transport, iron ion transport, and ferric iron binding significantly upregulated (Figure 4C) and DEGs highly enriched in TNF signaling pathway, mineral absorption, and ferroptosis (Figure 4D). The most NPs affected DEGs among the three cells was observed in HRs, with an average of 390 (Figure 2E). Using the DEGs to perform GO and KEGG enrichment analysis, we found that regulation of molecular function, cellular metabolic process, and protein modification process in HRs were significantly upregulated by NPs (Figure 4C), which might be highly enriched in NOD-like receptor signaling pathway (Figure 4D).

Fibroblasts were Identified as a Potential Sensitive Cell-Type Biomarker for MPs Interaction with *O. niloticus* Gills. Among the 12 cell types identified in *O. niloticus* gills, the most reduced cell counts were observed in MP-responsive FIBs, with 1726 FIBs inhibited (Figure 2D). Additionally, a total of 1227 DEGs were detected in the MP-responsive FIBs, sharing the highest number of DEGs as compared to other cell types (Figure 2E). Therefore, we supposed FIBs as a potential sensitive cell-type biomarker for MPs interaction with *O. niloticus* gills. The exclusively MP-responsive DEGs in FIBs were provided in Figure 5A, including *col1a1, col1a2, col6a1, col13a1, eif2a, dcn, pdgfra, dlx3, cops2,* and *deptor*, which could be considered as potential marker genes for future studies. The potential marker genes for NPs exposure can also be found in Figure 5A. The co-altered DEGs by MPs and NPs exposure are listed in Figure 5B. Based on the GO enrichment results, MPs exposure primarily downregulated activity of proton transmembrane transporter in FIBs, whereas NPs suppressed their vacuolar transport and carbohydrate derivative metabolic process (Figure 5C). Based on the KEGG enrichment results, the MP-responsive DEGs in FIBs were significantly enriched in HIF-1 signaling pathway and oxidative phosphorylation, whereas NP-responsive DEGs were mainly enriched in necroptosis (Figure 5D).

Fibroblasts Subpopulations of *O. niloticus* Gills Exhibited Different Expression Patterns to MPs and NPs. Unsupervised clustering was performed for FIBs in *O. niloticus* gills to distinguish their subpopulations. We obtained 12 FIB subclusters in total, sC0 through sC11 (Figure S10A), each containing unique marker genes (Figure S10B). The FIB subclusters were attributed to their putative identities based on the expression of classical markers (listed in Table S4). Specifically, sC3, sC6, and sC9 were identified as myofibroblasts (MYFs) due to their high enrichment of *col1a1* and *col1a2*. Wound healing fibroblasts (WHFs) were marked in sC2 FIB subcluster based on the high expression of *fn1a* and *fn1b*. Subclusters sC0, sC5, sC7, and sC8 were collectively classified as proinflammatory fibroblasts (PIFs) due to their high expression of *il6st*, *tnfaip6*, *mmp9*, and *cxcl14*. Lipofibroblasts (LPFs) were defined as such based on the high expression of *fabp7a* in sC1 and sC4. Due to the limited number of cells, sC10 and sC11 were discarded. The resulting cell atlas finally showed four FIB identities (Figure 6A), including MYFs, WHFs, PIFs, and LPFs, each containing 785, 998, 2,460, and 3,090 cells, respectively. Selective signature genes for each of the four FIB subpopulations are shown in Figure S11, providing potential markers for FIB subpopulation annotation in *O. niloticus* gills in future research. Cell numbers of the four FIB subpopulations were consistently reduced after MPs and NPs exposure and the reductions were uniformly more significant in the MP-treated group as compared to the NP-treated group (Figure 6B). However, the difference was that MPs exposure significantly disrupted the proportion of the four FIB subtypes by shifting the most dominant subpopulation from LPFs to PIFs, whereas MPs exposure did not induce similar changes (Figure S12). Additionally, significant cell number differences were consistently observed for the four FIB subpopulations between MPs and NPs exposure (Figure 6B). DEGs numbers of the four FIB subpopulations were consistently higher in the MP-treated group than in the NP-treated group (Figure 6D). However, the most detected DEGs among the four FIB subpopulations were different between MPs and NPs exposure, with an average of 1,723 (LPFs) and 176 (MYFs), respectively (Figure 6D). The expression levels of potential markers for each FIB subpopulation are depicted in Figure 6E.

MPs Disturbed Cell−Cell Communications Between Fibroblasts and Other Cell Populations in *O. niloticus* Gills. The impacts of MPs and NPs exposure on cellular communication between FIBs and the remaining 11 cell types in *O. niloticus* gills were investigated based on the average expression of the ligand–receptor pairs in different cell populations. The number of interactions between different cell populations in each group are

presented in Figure 7A. Based on the results of the control group, there existed closed cell−cell communications between FIBs and the remaining 11 cell populations in *O. niloticus* gills, particularly HRs, NERs, MAPs, NECs, and NaRs, with more than 20 ligand–receptor pairs significantly detected (Figure 7A). After MPs exposure, we found that the cell–cell interactions between FIBs and the remaining cell populations in *O. niloticus* gills were reduced to less than 10 (Figure 7A). However, the stimulus of NPs did not show significant changes for the cell−cell communications between FIBs and the remaining cell populations (Figure 7A). Among all the affected ligand–receptor pairs, CD74 interacted with MIF (Macrophage Migration Inhibitory Factor), COPA (Coatomer Protein Complex Subunit Alpha), and APP (Amyloid Precursor Protein) were the most sensitive ones in response to MPs (Figure 7B).

DISCUSSION

Fish breathe through their gills, the fine surface structures of which facilitates an effective exchange of oxygen and carbon dioxide and allows for a close contact with the water environment. [18] The high detected contents of AIE-MPs and AIE-NPs in *O. niloticus* gills highlight the importance of *O. niloticus* gills as a sensitive target organ for uptake of PS particles from the water environment. Although we did not analyze the contents of AIE-MPs and AIE-NPs in other tissues, recent studies reported that gills were among the major PS accumulated organs for fish. [16, 41] However, MPs and NPs accumulated differently and induced distinct morphological damages in *O. niloticus* gills. This was mainly because of the different behaviors of MPs and NPs when interacting with the gill microenvironment. It was speculated that MPs were more easily blocked or adhered on the epithelial surface for a long time and cause tissue physical damage herein, whereas NPs might be able to enter cells by penetrating biological membranes as an environmental insult in the circulatory system and interact with the cellular and subcellular components. [20, 42] In our study, scRNA-seq was conducted to investigate the transcriptional responses in *O. niloticus* gills at a single-cell resolution and compared the molecular mechanisms behind MPs and NPs. Based on the results of detected DEGs and cell number, MPs exposure generally induced higher transcriptional damages in *O. niloticus* gills compared to NPs exposure. This could well explain for the higher detected MPs contents in *O. niloticus* gills than NPs contents. However, such results contradicted the commonly accepted conclusion that smaller particle size led to higher toxicity [35] and indicated a high necessity to extensively investigate the

cellular heterogeneity responses induced by MPs and NPs.

Gills are important immune defense tissues for fish and play essential roles in their immune functions. [43] Four types of immune cells (TCs, MAPs, BCs, and NKCs) were successfully identified in *O. niloticus* gills. [40] These immune cells protect fish from infection and maintain their overall health by recognizing and clearing pathogens and xenobiotics. [44, 45] In previous studies, disturbed fish immune functions by MPs and NPs were widely recognized. [28, 46] Although MPs and NPs were expected to pose differential risks due to their disparities in cellular transport and fate, [47] their differences in immune functions were scarcely compared. Based on the detected DEGs, MAPs were highly sensitive to MPs exposure, but had no significant responses to NPs exposure. These results indicated that the stimulus of MPs in immune functions of *O. niloticus* gills might occur via attacking MAPs and inhibiting their respective immune functions. However, such mechanism was not applicable to the exposure of NPs. By contrast, among the four immune cells, NPs only induced high DEGs in TCs, suggesting that the major target immune cell for NPs stress was TCs, though similar responses were also observed in MPs-treated group. HRs, NaRs, and PVCs were the core cell populations responsible for distinct physiological functions of *O. niloticus*. [18] From the perspective of cell numbers, HRs exhibited contrasting changes with NaRs and PVCs following exposure to MPs and NPs, indicating their heterogeneous physiological responses. Regarding the detected DEGs, HRs were the most affected one among the three cell populations by NPs exposure. We therefore speculated that the stimulus of NPs mainly disturbed the regulation of acid-base balance, [40] while MPs did not show such heterogeneous responses.

Among the 12 identified cell populations in *O. niloticus* gills, FIBs were supposed as the most sensitive cell-type biomarker for MPs interaction with *O. niloticus* gills due to their largely reduced cell counts and mostly detected DEGs. Following injury, FIBs migrated towards the wound site and produce extracellular matrix (ECM) components to promote tissue regeneration. [48, 49] On this basis, we assumed the interaction of MPs with *O. niloticus* gills as a “wound to the skin”. It was commonly recognized that physical damages were the most direct impacts of MPs on organisms. [50, 51] Our results firstly unveiled the possible gene expression mechanisms behind the physical damages induced by MPs. In addition, FIBs are an extremely active cell type with diverse and dynamic functions. [52, 53] To our best knowledge, this is the first study to successfully characterize FIBs subpopulations in fish gills and investigate their heterogeneity responses to MPs. We further found that the most sensitive

FIBs subpopulation in *O. niloticus* gills was LPFs, which are a crucial subtype of FIBs responsible for structural support and cell-cell communication. [54] However, there were still some limitations for the proposed FIBs cell-type biomarker. Currently, we assumed this biomarker was conservatively suitable for specific fish species, tissue, MPs type, and MPs size employed in this study. Our findings provided significant insights into MPs biomarker investigation under broader conditions in future studies.

One of the most enriched KEGG pathway observed in MP-responsive FIBs was HIF-1 (hypoxia-inducible factor 1) signaling pathway (Figure S13), which normally represented a hypoxic stress state. [55] Gene expression profiles of respiratory damages in *O. niloticus* gills induced by MPs were demonstrated in previous studies by using bulk RNA-seq and the upregulation of gene *egln3* and *nadk* and downregulation of gene *cftr* might be the controlling mechanism. [20] This study further revealed cellular transcriptional responses for the respiratory damages observed in *O. niloticus* gills. The MPs-responsive respiratory damages in *O. niloticus* gills might be attribute to the upregulation of *ldha*, *aldoa*, *bcl2*, *hmox1*, *vegf*, *p300cbf*, *carnk*, *plcγ*, *pkc*, *pi3k*, *erk*, *4ebp1*, *rps6*, *hif1α*, *nfkb*, and *phd* in FIBs. Additionally, FIBs in *O. niloticus* gills are capable of synthesizing and releasing various signaling molecules, such as cytokines, growth factors, and cell adhesion molecules, [56] thereby communicating with surrounding cells and facilitating normal function. The significant inhibited cell-cell communications between FIBs and HRs, NERs, MAPs, NECs, NaRs by MPs need to be further investigated in future research.

This study used the advanced scRNA-seq technique to reveal the cellular heterogeneity responses of *O. niloticus* gills to MPs and NPs. Based on the results of cell numbers and/or detected DEGs, significant differences between MPs and NPs groups were observed for all the 12 identified cell populations of *O. niloticus* gills. FIBs were identified as a potential cell-type biomarker for MPs interaction with *O. niloticus* gills. Gene expression profiles of MPs-responsive FIBs provided possible mechanisms for the commonly recognized physical damages induced by MPs. The high enrichment of HIF-1 signaling pathway observed in MPs-responsive FIBs indicated respiratory damage at the single cell resolution. Overall, this study provided sensitive markers for understanding MPs and NPs toxicological mechanisms in fish.

Acknowledgement

We thank the anonymous reviewers for their helpful comments. This study was supported by

the Shenzhen Municipal Science and Technology Innovation Commission (JCYJ20220818101202006), and Hong Kong Research Grants Council (CityU 11103022) and the National Science Foundation of China (22276157).

Supporting information

Additional information as noted in the main text of the current paper is available, including Texts S1–S2, Figures S1–S13, and Tables S1–S3.
Calculation details of AIE-MPs and AIE-NPs contents in *O. niloticus* gills (Text S1); Methods of histopathological analysis (Text S2); Comparison between fluorescence intensity of the commercial PS and AIE-PS (Figure S1); Concentration of AIE-MPs and AIE-NPs suspension during exposure (Figure S2); Representative H&E sections (Figure S3); UMAP plot showing 33 clusters (Figure S4A); Heatmap plot showing the top 3 enriched genes per cluster (Figure S4B); Heatmap plot showing the top 10 enriched genes per cell population (Figure S5A); Violin plots showing expression of signature genes (Figure S5B); UMAP plot showing 33 clusters per condition (Figure S6); Total cell number per sample per condition (Figure S7); Volcano map showing DEGs per condition based on bulk RNA sequencing (Figure S8); Integrated comparative analysis of DEGs among cell populations (Figure S9); UMAP plot showing 12 FIB subclusters (Figure S10A); Heatmap plot showing the top 10 enriched genes per FIB subcluster (Figure S10B); Expression of signature genes of the four FIB subpopulations (Figure S11); Cell proportion of the four FIB subpopulations (Figure S12); Predicted diagram of HIF-1 signaling pathway (Figure S13); Body length and weight of *O. niloticus* (Table S1); Sequence alignment analysis (Table S2); Markers used for cell population annotation (Table S3); Markers used for FIB subpopulation annotation (Table S4).

REFERENCES

(1) Hussain, K. A.; Romanova, S.; Okur, I.; Zhang, D.; Kuebler, J.; Huang, X.; Wang, B.; Fernandez-Ballester, L.; Lu, Y.; Schubert, M.; Li, Y. Assessing the release of microplastics and nanoplastics from plastic containers and reusable food pouches: Implications for human health. *Environ. Sci. Technol.* **2023**, *57* (26), 9782-9792.

(2) Li, D.; Shi, Y.; Yang, L.; Xiao, L.; Kehoe, D. K.; Gun'ko, Y. K.; Boland, J. J.; Wang, J. J. Microplastic release from the degradation of polypropylene feeding bottles during infant formula preparation. *Nat. Food* **2020**, *1* (11), 746-754.

(3) Yadav, H.; Khan, M. R. H.; Quadir, M.; Rusch, K. A.; Mondal, P. P.; Orr, M.; Xu, E. G.; Iskander, S. M. Cutting boards: An overlooked source of microplastics in human food? *Environ. Sci. Technol.* **2023**, *57* (22), 8225-8235.

(4) Wang, W.-X. Environmental toxicology of marine microplastic pollution. *Cambridge Prisms: Plastics* **2023**, *1*, e10.

(5) Borrelle, S. B.; Ringma, J.; Law, K. L.; Monnahan, C. C.; Lebreton, L.; McGivern, A.; Murphy, E.; Jambeck, J.; Leonard, G. H.; Hilleary, M. A.; Eriksen, M.; Possingham, H. P.; De Frond, H.; Gerber, L. R.; Polidoro, B.; Tahir, A.; Bernard, M.; Mallos, N.; Barnes, M.; Rochman, C. M. Predicted growth in plastic waste exceeds efforts to mitigate plastic pollution. *Science* **2020**, *369* (6510), 1515-1518.

(6) Neves, D.; Sobral, P.; Ferreira, J. L.; Pereira, T. Ingestion of microplastics by commercial fish off the Portuguese coast. *Mar. Pollut. Bull.* **2015**, *101* (1), 119-126.

(7) Braun, T.; Ehrlich, L.; Henrich, W.; Koeppel, S.; Lomako, I.; Schwabl, P.; Liebmann, B. Detection of microplastic in human placenta and meconium in a clinical setting. *Pharmaceutics* **2021**, *13* (7), 921.

(8) Yan, Z.; Liu, Y.; Zhang, T.; Zhang, F.; Ren, H.; Zhang, Y. Analysis of microplastics in human feces reveals a correlation between fecal microplastics and inflammatory bowel disease status. *Environ. Sci. Technol.* **2022**, *56* (1), 414-421.

(9) Dawson, A. L.; Kawaguchi, S.; King, C. K.; Townsend, K. A.; King, R.; Huston, W. M.; Bengtson Nash, S. M. Turning microplastics into nanoplastics through digestive fragmentation by Antarctic krill. *Nat. Commun.* **2018**, *9* (1), 1001.

(10) Teng, M.; Zhao, X.; Wang, C.; Wang, C.; White, J. C.; Zhao, W.; Zhou, L.; Duan, M.; Wu, F. Polystyrene Nanoplastics Toxicity to Zebrafish: Dysregulation of the Brain-Intestine-Microbiota Axis. *ACS Nano* **2022**, *16* (5), 8190-8204.

(11) Lin, W.; Luo, H.; Wu, J.; Liu, X.; Cao, B.; Liu, Y.; Yang, P.; Yang, J. Polystyrene microplastics enhance the microcystin-LR-induced gonadal damage and reproductive endocrine disruption in zebrafish. *Sci. Total Environ.* **2023**, *876*, 162664.

(12) Hu, J.; Zuo, J.; Li, J.; Zhang, Y.; Ai, X.; Zhang, J.; Gong, D.; Sun, D. Effects of secondary polyethylene microplastic exposure on crucian (*Carassius carassius*) growth, liver damage, and gut microbiome composition. *Sci. Total Environ.* **2022**, *802*, 149736.

(13) Li, W.; Chen, X.; Li, M.; Cai, Z.; Gong, H.; Yan, M. Microplastics as an aquatic pollutant affect gut microbiota within aquatic animals. *J. Hazard. Mater.* **2022**, *423*, 127094.

(14) Yang, L.; Tang, B. Z.; Wang, W.-X. Near-infrared-II *in vivo* visualization and quantitative tracking of micro/nanoplastics in fish. *ACS Nano* **2023**, *17* (19), 19410-19420.

(15) Jin, Y.; Xia, J.; Pan, Z.; Yang, J.; Wang, W.; Fu, Z. Polystyrene microplastics induce microbiota dysbiosis and inflammation in the gut of adult zebrafish. *Environ. Pollut.* **2018**,

582 *235*, 322-329.
583 (16) Yeo, I.-C.; Shim, K.-Y.; Kim, K.; Go, Y.-S.; Kim, J.; Lee, D.-H.; Lee, J.-S.; Shin, K.-H.;
584 Jeong, C.-B. Insights into tissue-specific bioaccumulation of nanoplastics in marine medaka
585 as revealed by a stable carbon isotopic approach. *Environ. Sci. Technol. Lett.* **2023**, *10* (10),
586 838-843.
587 (17) Ivanova, L.; Rangel-Huerta, O. D.; Tartor, H.; Gjessing, M. C.; Dahle, M. K.; Uhlig, S.
588 Fish skin and gill mucus: a source of metabolites for non-invasive health monitoring and
589 research. *Metabolites* **2021**, *12* (1), 28.
590 (18) Evans, D. H.; Piermarini, P. M.; Choe, K. P. The multifunctional fish gill: Dominant site
591 of gas exchange, osmoregulation, acid-base regulation, and excretion of nitrogenous waste.
592 *Physiol. Rev.* **2005**, *85* (1), 97-177.
593 (19) Zheng, S.; Wang, W.-X. Disturbing ion regulation and excretion in medaka (*Oryzias*
594 *melastigma*) gills by microplastics: Insights from the gut-gill axis. *Sci. Total Environ.* **2023**,
595 *857*, 159353.
596 (20) Zheng, S.; Tang, B. Z.; Wang, W.-X. Microplastics and nanoplastics induced differential
597 respiratory damages in tilapia fish *Oreochromis niloticus*. *J. Hazard. Mater.* **2024**, *465*,
598 133181.
599 (21) Meng, J.; Wang, W.-X. Highly sensitive and specific responses of oyster hemocytes to
600 copper exposure: Single-cell transcriptomic analysis of different cell populations. *Environ.*
601 *Sci. Technol.* **2022**, *56* (4), 2497-2510.
602 (22) Ge, Q.; Wang, J.; Li, J.; Li, J. Highly sensitive and specific responses of shrimp gill cells
603 to high pH stress based on single cell RNA-seq analysis. *Front. Cell Dev. Biol.* **2022**, *10*,
604 1031828.
605 (23) LeMoine, C. M.; Kelleher, B. M.; Lagarde, R.; Northam, C.; Elebute, O. O.; Cassone, B.
606 J. Transcriptional effects of polyethylene microplastics ingestion in developing zebrafish
607 (*Danio rerio*). *Environ. Pollut.* **2018**, *243*, 591-600.
608 (24) Cuesta, A.; Espinosa, C.; Esteban, M. A.; González-Fernández, C. Application of
609 transcriptomic profiling to investigate the toxicity mechanisms caused by dietary exposure of
610 nanoplastics in fish. *Aquat. Toxicol.* **2023**, *264*, 106712.
611 (25) Segerstolpe, Å.; Palasantza, A.; Eliasson, P.; Andersson, E.-M.; Andréasson, A.-C.; Sun,
612 X.; Picelli, S.; Sabirsh, A.; Clausen, M.; Bjursell, M. K. Single-cell transcriptome profiling of
613 human pancreatic islets in health and type 2 diabetes. *Cell metab.* **2016**, *24* (4), 593-607.
614 (26) Xie, X.; Shi, Q.; Wu, P.; Zhang, X.; Kambara, H.; Su, J.; Yu, H.; Park, S.-Y.; Guo, R.;
615 Ren, Q.; Zhang, S.; Xu, Y.; Silberstein, L. E.; Cheng, T.; Ma, F.; Li, C.; Luo, H. R. Single-cell
616 transcriptome profiling reveals neutrophil heterogeneity in homeostasis and infection. *Nat.*
617 *Immunol.* **2020**, *21* (9), 1119-1133.
618 (27) Chen, L.; Wang, Z.; Gu, W.; Zhang, X.-X.; Ren, H.; Wu, B. Single-cell sequencing
619 reveals heterogeneity effects of bisphenol A on zebrafish embryonic development. *Environ.*
620 *Sci. Technol.* **2020**, *54* (15), 9537-9546.
621 (28) Gu, W.; Liu, S.; Chen, L.; Liu, Y.; Gu, C.; Ren, H.-Q.; Wu, B. Single-Cell RNA
622 sequencing reveals size-dependent effects of polystyrene microplastics on immune and
623 secretory cell populations from zebrafish intestines. *Environ. Sci. Technol.* **2020**, *54* (6),
624 3417-3427.
625 (29) Gigault, J.; El Hadri, H.; Nguyen, B.; Grassl, B.; Rowenczyk, L.; Tufenkji, N.; Feng, S.;

Wiesner, M. Nanoplastics are neither microplastics nor engineered nanoparticles. *Nat. Nano.* **2021**, *16* (5), 501-507.
(30) Wang, H.; Li, Q.; Alam, P.; Bai, H.; Bhalla, V.; Bryce, M. R.; Cao, M.; Chen, C.; Chen, S.; Chen, X.; Chen, Y.; Chen, Z.; Dang, D.; Ding, D.; Ding, S.; Duo, Y.; Gao, M.; He, W.; He, X.; Hong, X.; Hong, Y.; Hu, J.-J.; Hu, R.; Huang, X.; James, T. D.; Jiang, X.; Konishi, G.-i.; Kwok, R. T. K.; Lam, J. W. Y.; Li, C.; Li, H.; Li, K.; Li, N.; Li, W.-J.; Li, Y.; Liang, X.-J.; Liang, Y.; Liu, B.; Liu, G.; Liu, X.; Lou, X.; Lou, X.-Y.; Luo, L.; McGonigal, P. R.; Mao, Z.-W.; Niu, G.; Owyong, T. C.; Pucci, A.; Qian, J.; Qin, A.; Qiu, Z.; Rogach, A. L.; Situ, B.; Tanaka, K.; Tang, Y.; Wang, B.; Wang, D.; Wang, J.; Wang, W.; Wang, W.-X.; Wang, W.-J.; Wang, X.; Wang, Y.-F.; Wu, S.; Wu, Y.; Xiong, Y.; Xu, R.; Yan, C.; Yan, S.; Yang, H.-B.; Yang, L.-L.; Yang, M.; Yang, Y.-W.; Yoon, J.; Zang, S.-Q.; Zhang, J.; Zhang, P.; Zhang, T.; Zhang, X.; Zhang, X.; Zhao, N.; Zhao, Z.; Zheng, J.; Zheng, L.; Zheng, Z.; Zhu, M.-Q.; Zhu, W.-H.; Zou, H.; Tang, B. Z. Aggregation-induced emission (AIE), life and health. *ACS Nano* **2023**, *17* (15), 14347-14405.
(31) Yan, N.; Tang, B. Z.; Wang, W.-X. Cell cycle control of nanoplastics internalization in phytoplankton. *ACS Nano* **2021**, *15* (7), 12237-12248.
(32) Wang, M.; Wang, W.-X. Accumulation kinetics and gut microenvironment responses to environmentally relevant doses of micro/nanoplastics by zooplankton *Daphnia magna*. *Environ. Sci. Technol.* **2023**, *57* (14), 5611-5620.
(33) Sun, X.-D.; Yuan, X.-Z.; Jia, Y.; Feng, L.-J.; Zhu, F.-P.; Dong, S.-S.; Liu, J.; Kong, X.; Tian, H.; Duan, J.-L.; Ding, Z.; Wang, S.-G.; Xing, B. Differentially charged nanoplastics demonstrate distinct accumulation in *Arabidopsis thaliana*. *Nat. Nanotechnol.* **2020**, *15* (9), 755-760.
(34) Xu, S.; Wu, C.; Guo, W.-B.; Yang, L.; Ji, R.; Pan, K.; Miao, A.-J. Polystyrene nanoplastics inhibit the transformation of tetrabromobisphenol A by the bacterium *Rhodococcus jostii*. *ACS Nano* **2022**, *16* (1), 405-414.
(35) Li, Z.; Feng, C.; Pang, W.; Tian, C.; Zhao, Y. Nanoplastic-Induced genotoxicity and intestinal damage in freshwater benthic clams (*Corbicula fluminea*): Comparison with microplastics. *ACS Nano* **2021**, *15* (6), 9469-9481.
(36) Dusaucy, J.; Gateuille, D.; Perrette, Y.; Naffrechoux, E. Microplastic pollution of worldwide lakes. *Environ. Pollut.* **2021**, *284*, 117075.
(37) OECD. Test No. 210: Fish, early-life stage toxicity test. **2013**.
(38) Liu, Y.; Zuo, X.; Chen, P.; Hu, X.; Sheng, Z.; Liu, A.; Liu, Q.; Leng, S.; Zhang, X.; Li, X.; Wang, L.; Feng, Q.; Li, C.; Hou, M.; Chu, C.; Ma, S.; Wang, S.; Peng, J. Deciphering transcriptome alterations in bone marrow hematopoiesis at single-cell resolution in immune thrombocytopenia. *Signal Transduct. Target Ther.* **2022**, *7* (1), 347.
(39) He, X.; Smith, S. E.; Chen, S.; Li, H.; Wu, D.; Meneses-Giles, P. I.; Wang, Y.; Hembree, M.; Yi, K.; Zhao, X. Tumor-initiating stem cell shapes its microenvironment into an immunosuppressive barrier and pro-tumorigenic niche. *Cell Rep.* **2021**, *36* (10).
(40) Zheng, S.; Wang, W.-X. Physiological and immune profiling of tilapia *Oreochromis niloticus* gills by high-throughput single-cell transcriptome sequencing. *Fish Shellfish Immunol.* **2023**, 109070.
(41) Hao, T.; Gao, Y.; Li, Z.-C.; Zhou, X.-X.; Yan, B. Size-dependent uptake and depuration of nanoplastics in tilapia (*Oreochromis niloticus*) and distinct intestinal impacts. *Environ. Sci.*

Technol. **2023**, *57* (7), 2804-2812.
(42) Yin, K.; Wang, Y.; Zhao, H.; Wang, D.; Guo, M.; Mu, M.; Liu, Y.; Nie, X.; Li, B.; Li, J.; Xing, M. A comparative review of microplastics and nanoplastics: Toxicity hazards on digestive, reproductive and nervous system. *Sci. Total Environ.* **2021**, *774*, 145758.
(43) Press, C. M.; Evensen, Ø. The morphology of the immune system in teleost fishes. *Fish Shellfish Immunol.* **1999**, *9* (4), 309-318.
(44) Nakanishi, T.; Shibasaki, Y.; Matsuura, Y. T cells in fish. *Biology* **2015**, *4* (4), 640-663.
(45) Fischer, U.; Koppang, E. O.; Nakanishi, T. Teleost T and NK cell immunity. *Fish Shellfish Immunol.* **2013**, *35* (2), 197-206.
(46) Huang, J. N.; Wen, B.; Zhu, J. G.; Zhang, Y. S.; Gao, J. Z.; Chen, Z. Z. Exposure to microplastics impairs digestive performance, stimulates immune response and induces microbiota dysbiosis in the gut of juvenile guppy (*Poecilia reticulata*). *Sci. Total Environ.* **2020**, *733*, 138929.
(47) Peijnenburg, W. J.; Baalousha, M.; Chen, J.; Chaudry, Q.; Von der kammer, F.; Kuhlbusch, T. A.; Lead, J.; Nickel, C.; Quik, J. T.; Renker, M. A review of the properties and processes determining the fate of engineered nanomaterials in the aquatic environment. *Crit. Rev. Environ. Sci. Technol.* **2015**, *45* (19), 2084-2134.
(48) Guerrero-Juarez, C. F.; Dedhia, P. H.; Jin, S.; Ruiz-Vega, R.; Ma, D.; Liu, Y.; Yamaga, K.; Shestova, O.; Gay, D. L.; Yang, Z.; Kessenbrock, K.; Nie, Q.; Pear, W. S.; Cotsarelis, G.; Plikus, M. V. Single-cell analysis reveals fibroblast heterogeneity and myeloid-derived adipocyte progenitors in murine skin wounds. *Nat. Commun.* **2019**, *10* (1), 650.
(49) Talbott, H. E.; Mascharak, S.; Griffin, M.; Wan, D. C.; Longaker, M. T. Wound healing, fibroblast heterogeneity, and fibrosis. *Cell Stem Cell* **2022**, *29* (8), 1161-1180.
(50) Ahrendt, C.; Perez-Venegas, D.; Urbina, M.; Gonzalez, C.; Echeveste, P.; Aldana, M.; Pulgar, J.; Galbán-Malagón, C. Microplastic ingestion cause intestinal lesions in the intertidal fish *Girella laevifrons*. *Mar. Pollut. Bull.* **2020**, *151*, 110795.
(51) Peda, C.; Caccamo, L.; Fossi, M. C.; Gai, F.; Andaloro, F.; Genovese, L.; Perdichizzi, A.; Romeo, T.; Maricchiolo, G. Intestinal alterations in European sea bass *Dicentrarchus labrax* (Linnaeus, 1758) exposed to microplastics: Preliminary results. *Environ. Pollut.* **2016**, *212*, 251-256.
(52) Griffin, M. F.; desJardins-Park, H. E.; Mascharak, S.; Borrelli, M. R.; Longaker, M. T. Understanding the impact of fibroblast heterogeneity on skin fibrosis. *Dis. Model. Mech.* **2020**, *13* (6).
(53) Deng, C.-C.; Hu, Y.-F.; Zhu, D.-H.; Cheng, Q.; Gu, J.-J.; Feng, Q.-L.; Zhang, L.-X.; Xu, Y.-P.; Wang, D.; Rong, Z. Single-cell RNA-seq reveals fibroblast heterogeneity and increased mesenchymal fibroblasts in human fibrotic skin diseases. *Nat. Commun.* **2021**, *12* (1), 3709.
(54) Schipke, J.; Kuhlmann, S.; Hegermann, J.; Fassbender, S.; Kühnel, M.; Jonigk, D.; Mühlfeld, C. Lipofibroblasts in structurally normal, fibrotic, and emphysematous human lungs. *Am. J. Resp. Crit. Care* **2021**, *204* (2), 227-230.
(55) Semenza, G. L. HIF-1 and mechanisms of hypoxia sensing. *Curr. Opin. Cell Biol.* **2001**, *13* (2), 167-171.
(56) Eswarakumar, V.; Lax, I.; Schlessinger, J. Cellular signaling by fibroblast growth factor receptors. *Cytokine Growth Factor Rev.* **2005**, *16* (2), 139-149.

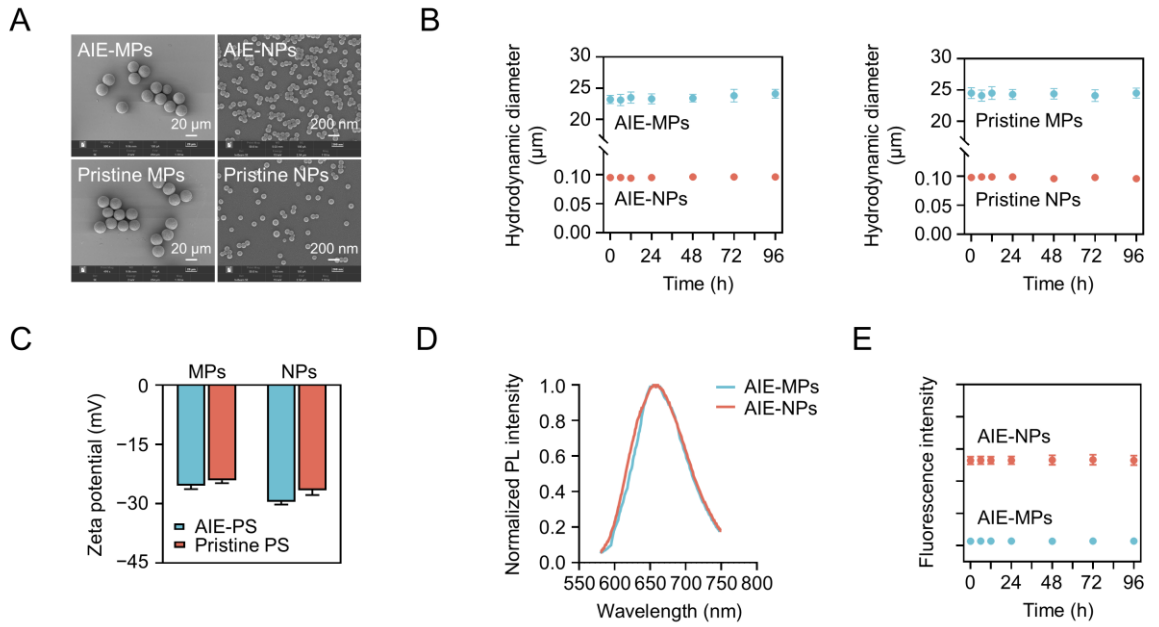

Figure 1. Characterization of MPs and NPs. (A) Scanning electron microscopy images. (B) Hydrodynamic diameters in culture water over 96 consecutive hours. (C) Zeta potentials. (D) Normalized photoluminescence (PL) spectra of the synthesized AIE-MPs and AIE-NPs (excitation 510 nm; emission 655 nm). (E) Stability of the fluorescence signal emitted from the AIE-MPs and AIE-NPs over 96 consecutive hours.

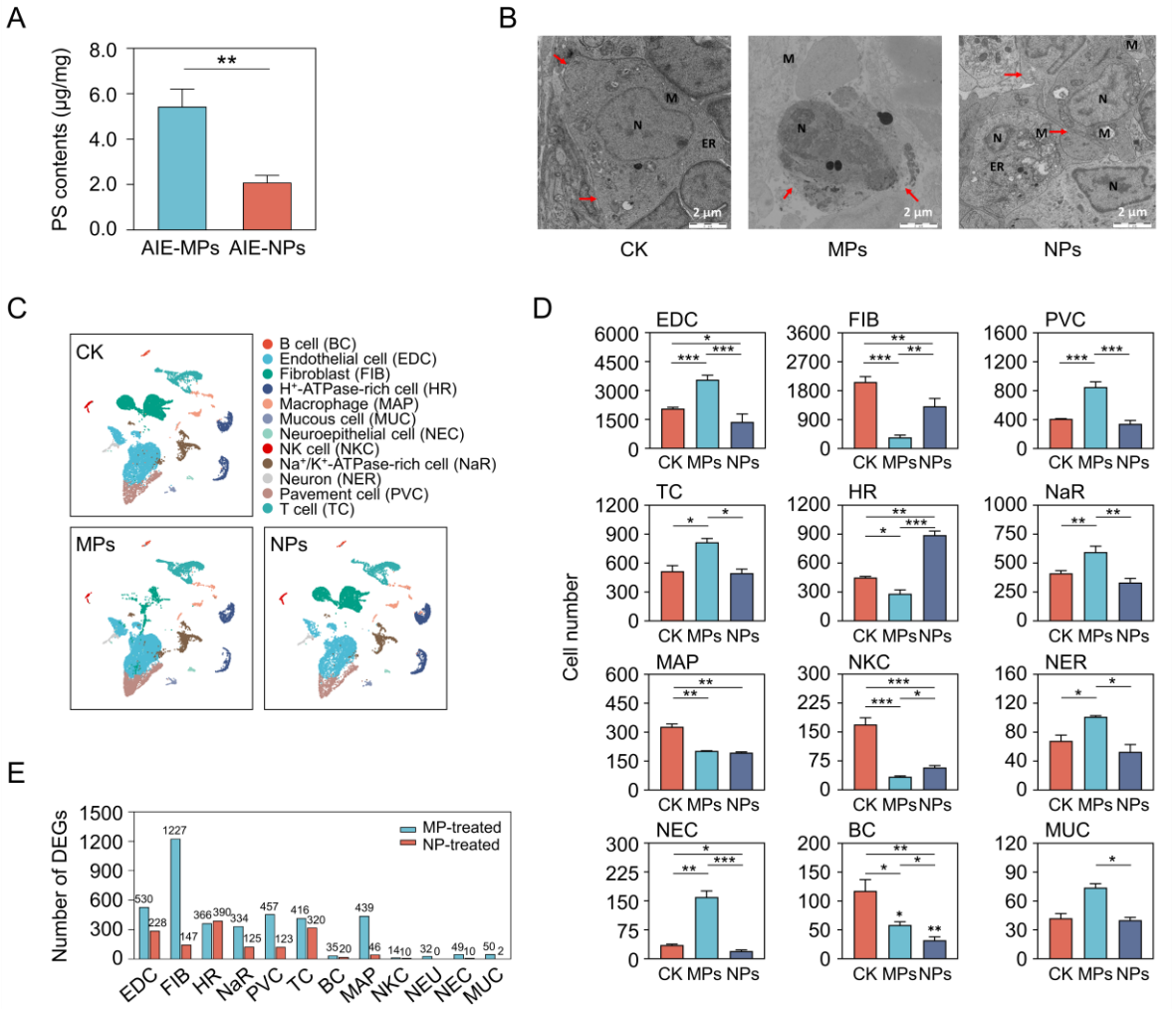

Figure 2. (A) Corrected AIE-MPs and AIE-NPs contents in gills of *O. niloticus* after 28-day exposure. Asterisks indicate significant differences (** $p < 0.01$) between the two treatments. (B) TEM images of *O. niloticus* gills in control, MP-treated, and NP-treated groups. N represents cell nucleus; M represents mitochondria; ER represents endoplasmic reticulum; red arrow represents cell membrane. (C) UMAP plots of the 12 cell populations of *O. niloticus* gills in control, MP-treated, and NP-treated groups. (D) Number of the 12 cell populations of *O. niloticus* gills in control, MP-treated, and NP-treated groups. Asterisks indicate significant differences (* $p < 0.05$, ** $p < 0.01$, and *** $p < 0.001$) between the treatments and the control group. (E) Number of the differentially expressed genes (DEGs) in the 12 cell populations of *O. niloticus* gills under MP-treated and NP-treated conditions.

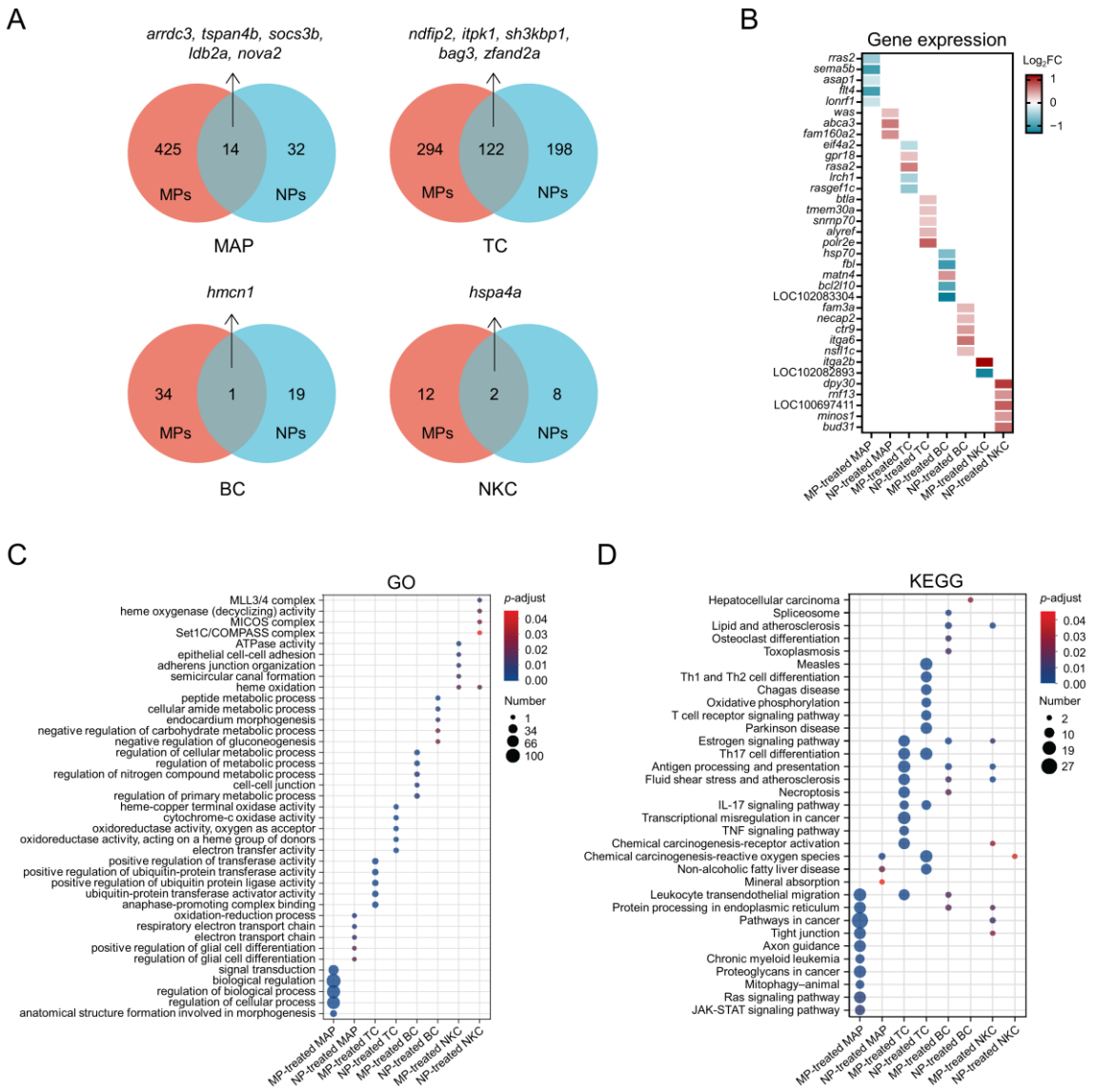

Figure 3. Transcriptional profiles of the four immune cells (MAPs, TCs, BCs, and NKCs) in *O. niloticus* gills in MP-treated and NP-treated groups. (A) Integrated comparative analysis. (B) A heatmap representing expression patterns of selective DEGs. Representative (C) Gene Ontology (GO) terms and (D) Kyoto Encyclopedia of Genes and Genomes (KEGG) pathways. FC, fold change.

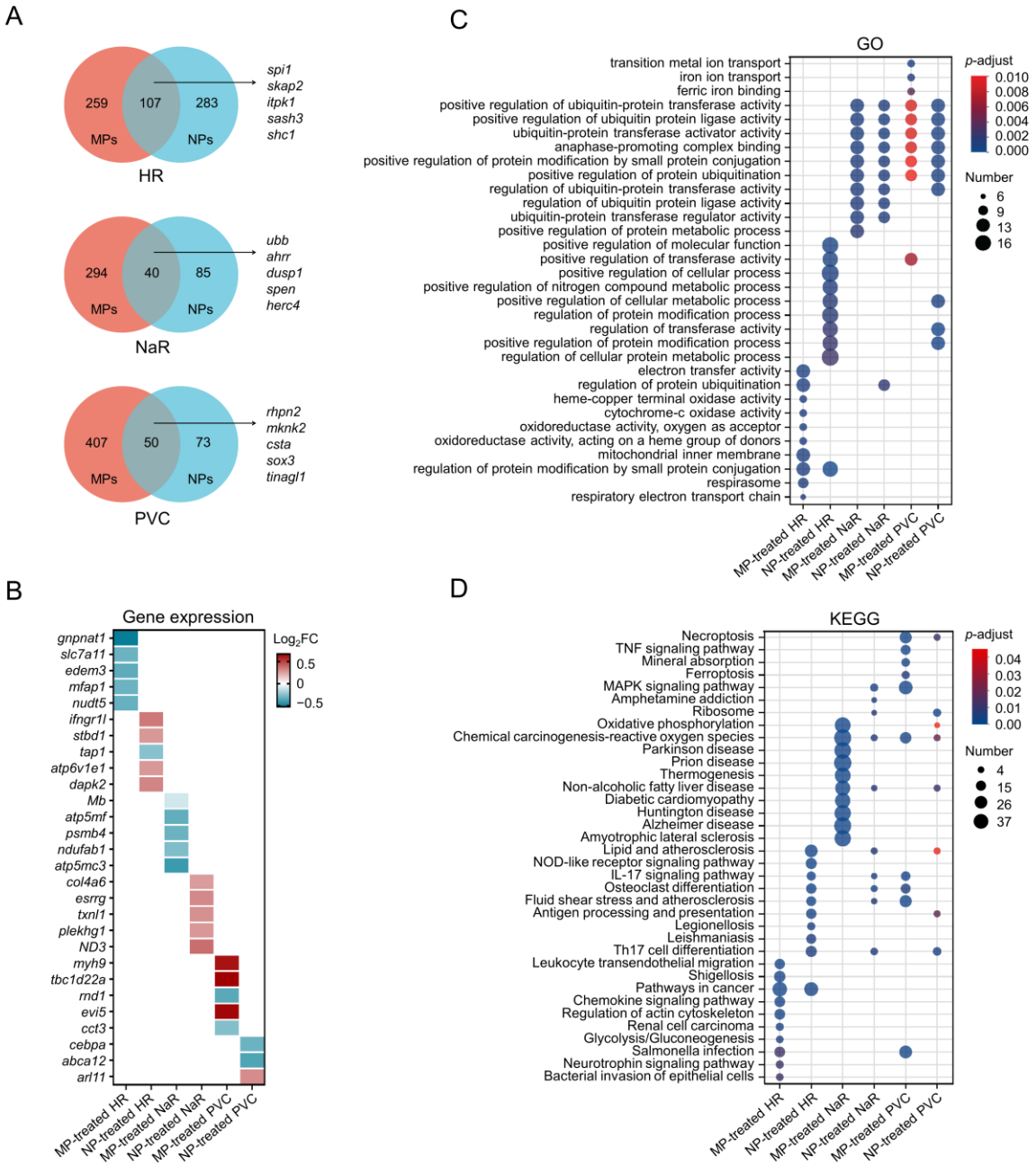

Figure 4. Transcriptional profiles of HRs, NaRs, and PVCs in *O. niloticus* gills in MP-treated and NP-treated groups. (A) Integrated comparative analysis of DEGs. (B) A heatmap representing expression patterns of selective DEGs. Representative (C) GO terms and (D) KEGG pathways.

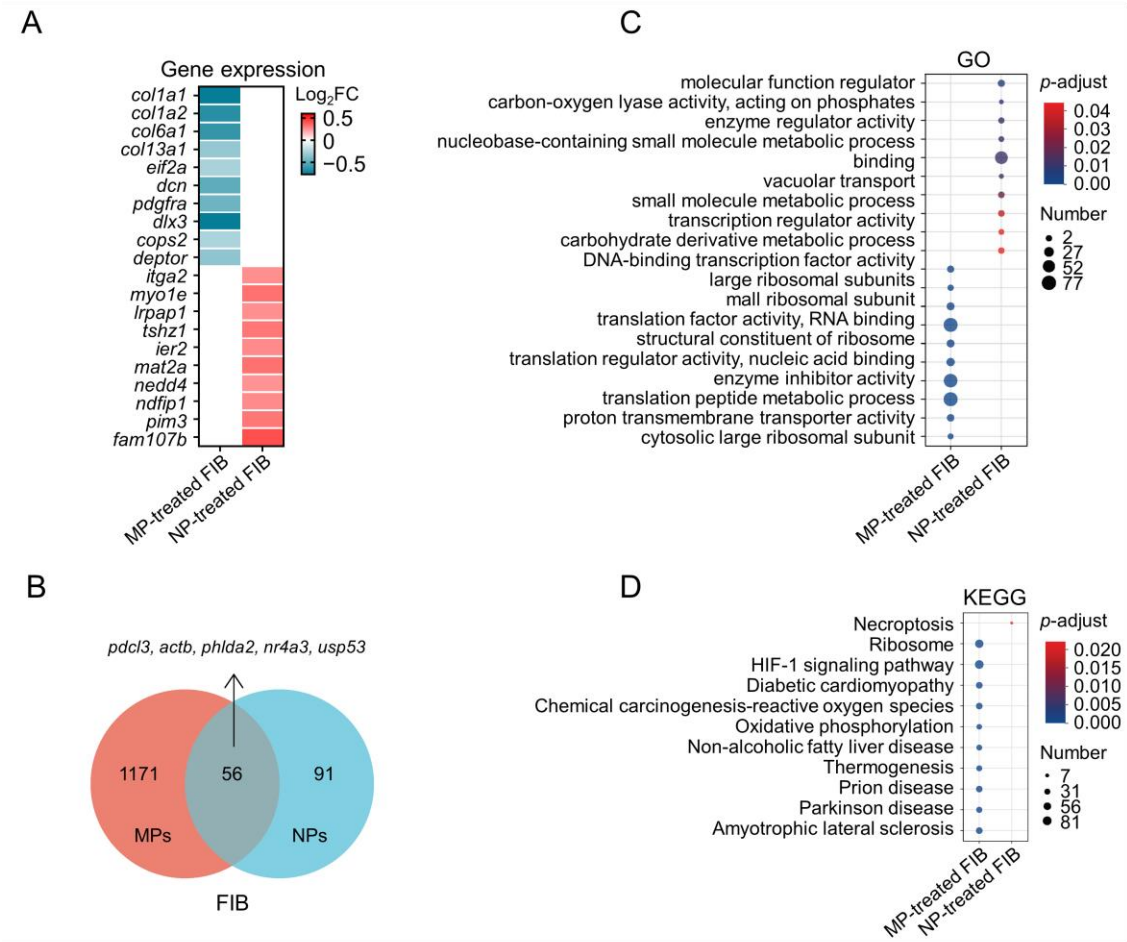

Figure 5. Transcriptional profiles of FIBs in *O. niloticus* gills in MP-treated and NP-treated groups. (A) A heatmap representing expression patterns of selective DEGs. (B) Integrated comparative analysis of DEGs. Representative (C) GO terms and (D) KEGG pathways.

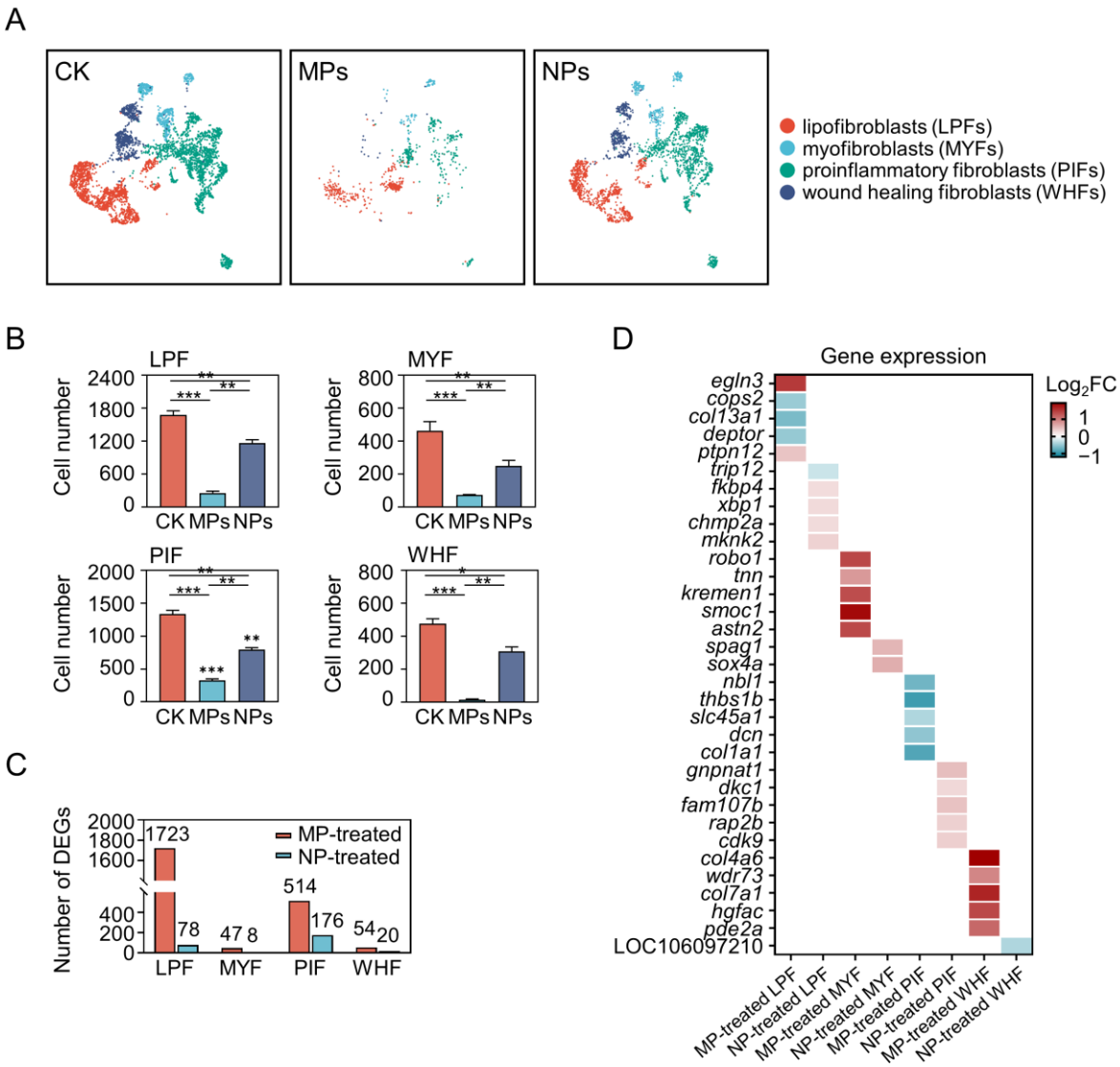

Figure 6. Transcriptional profiles of FIB subpopulations in *O. niloticus* gills. (A) UMAP plots in control, MP-treated, and NP-treated groups. (B) Cell numbers in control, MP-treated, and NP-treated groups. Asterisks indicate significant differences (* $p < 0.05$, ** $p < 0.01$, and *** $p < 0.001$) between the treatments and the control group. (C) Number of DEGs under MP-treated and NP-treated conditions. (D) A heatmap representing expression patterns of selective DEGs under MP-treated and NP-treated conditions.

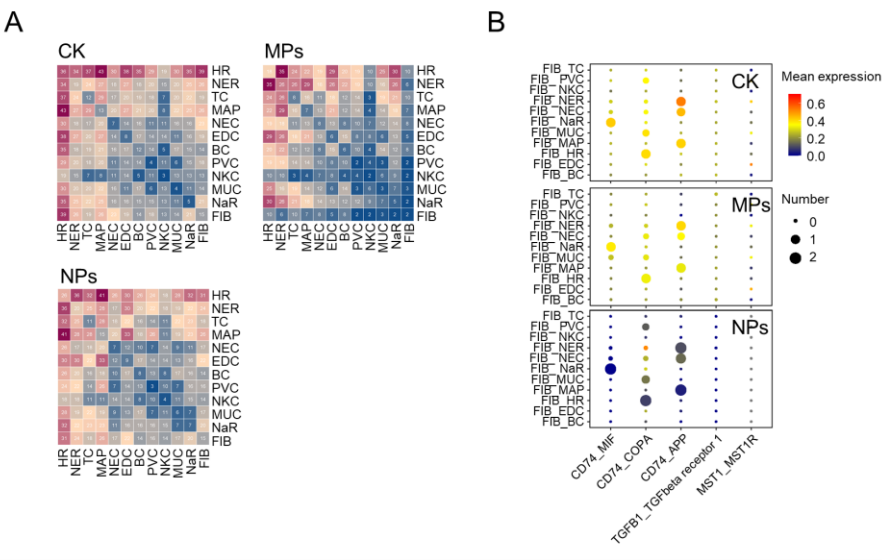

753
754 Figure 7. Cell−cell communications among the 12 cell populations of *O. niloticus* gills in
755 control, MP-treated, and NP-treated groups. (A) A heatmap representing number of
756 ligand−receptor pairs. The blue color indicates fewer ligand−receptor pairs; the purple color
757 indicates more ligand−receptor pairs. (B) Expression levels of selective ligand−receptor
758 pairs.